CRYSTAL GROWTH & DESIGN

pubs.acs.org/crystal

Perspective

Atomic Layer Deposition of Transition-Metal Dichalcogenides

Zhipu Li, Xun Zhao, Shiru Wu, Min Lu, Xiaoji Xie, and Jiaxu Yan*

Cite This: *Cryst. Growth Des.* 2024, 24, 1865−1879

Read Online

ACCESS | Metrics & More | Article Recommendations

ABSTRACT: Two-dimensional (2D) transition metal sulfides (TMDs) semiconductors, represented by MoS_2, are regarded as promising candidates to advance Moore's law in the postsilicon semiconductor era, as they possess the advantages of high carrier mobility, high switching ratios, tunable bandgap, and atomic-level thickness, as well as combining with good mechanical properties. The exploration of high-quality large-area 2D materials is crucial for investigating new physical phenomena and further extending their applications in microelectronics and optoelectronics. Among the techniques for producing high-quality 2D materials, atomic layer deposition (ALD) stands out as a self-limiting surface chemical reaction-based method. It offers more advantages in terms of step coverage, wafer size uniformity, and controllable stoichiometric ratio, which is expected to overcome the bottleneck in the utilization of 2D materials in optoelectronic integrated devices and future large-scale applications. In this paper, we provide an overview of the structure and properties of TMDs, and then focus on the latest progress in the ALD-based preparation of TMD thin films. Key factors influencing the film quality are discussed, and we conclude by discussing the potential future development trends in this field.

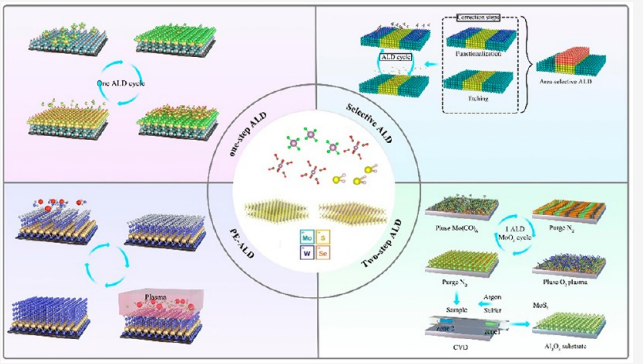

1. INTRODUCTION

Two-dimensional (2D) transition-metal dichalcogenides (TMDs), characterized by MX_2 layered structure (M: transition metals, X: sulfur group elements), have garnered substantial research attention. Unlike graphene, numerous 2D TMDs inherently function as semiconductors, boasting attributes such as remarkable carrier mobility, tunable bandgap, ultrathin dimensions, uniform surfaces devoid of dangling bonds, and compatibility with flexible substrates.[1−6] This enables the creation of compact, energy-efficient optoelectronic devices with heightened efficiency, offering a wide scope for integration across diverse applications. The distinctive electrical and optical traits of 2D TMDs arise from quantum confinement and surface effects, manifesting as the transition from an indirect to a direct bandgap when bulk material condenses into a monolayer. This tunable bandgap accompanies robust photoluminescence (PL) and substantial exciton binding energy, presenting promising avenues in optoelectronics, encompassing solar cells,[7,8] photodetectors,[9,10] light-emitting diodes (LEDs),[11,12] and phototransistors.[13]

Figure 1 illustrates layered TMDs, with each unit cell (MX_2) containing a transition metal (M) layer sandwiched between two sulfur (X) atom layers. The atomic configuration classifies TMD structures into hexagonal (H) and octahedral (or tetrahedral, T) phases, along with distorted T′ phases. In the H-phase, metal atoms extend in the $+z$ and $-z$ directions, forming two tetrahedra, while the top view displays hexagonal symmetry. The arrangement of sulfur−metal−sulfur elements in the z-direction constitutes a monolayer, held together by weak van der Waals interactions, facilitating mechanical exfoliation from bulk TMDs into monolayer flakes. The T-phase features a top layer of sulfur atoms and a 180-degree rotated bottom structure (triangular antiprism). At room temperature, the stable 2H phase exhibits higher conductivity than the chemically stripped metallic 1T phase in MoS_2. Similarly, WTe_2 shows stability of the 1T or 1T′ phase over the 2H phase at room temperature. $MoTe_2$'s 2H and 1T′ phases, with similar cohesion energy differences, allow convenient modulation between the two phases.

Achieving defect-free, large-scale atomic layers of 2D TMDs with adjustable thicknesses on custom substrates remains a challenge despite their unique properties compared to conventional bulk materials or thin films. TMDs, including 2D layers, can be synthesized through top-down methods (mechanical exfoliation, chemical liquid-phase exfoliation, etc.)

Received: September 1, 2023
Revised: December 12, 2023
Accepted: December 12, 2023
Published: January 4, 2024

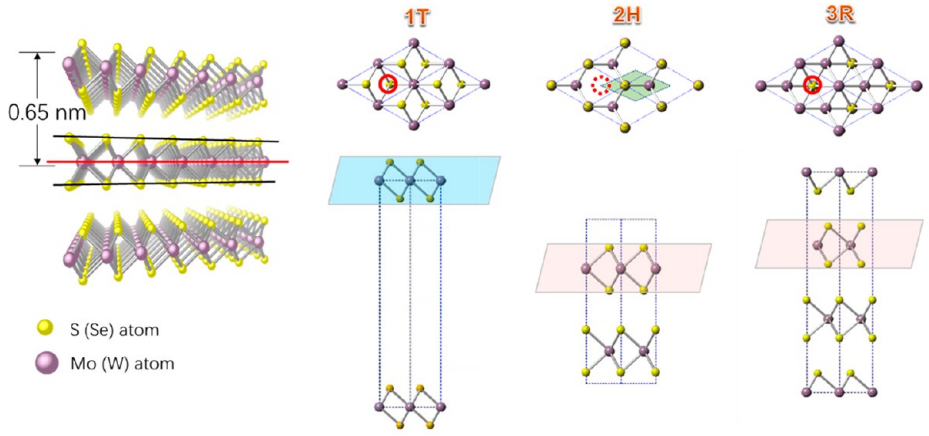

Figure 1. Side view of the MoS_2 crystal structure and typical phases with various stacking.

Table 1. Summary of TMD Films Synthesized via Various ALD Processes

TMD	Precursor A	Precursor B	Growth Temperature (°C)	Substrate	Program[a]	References
MoS_2	$MoCl_5$	H_2S	300	Al_2O_3	P1	48
	$MoCl_5$	H_2S	350−450	Si/SiO_2	P1	49
	$MoCl_5$	HMDST		Si/SiO_2, Al_2O_3	P1	51
	$MoCl_5$	H_2S	430−470	Si/SiO_2, Al_2O_3	P1	36
	$C_8H_{24}MoN_4$	CH_3SSCH_3	60	Al_2O_3	P1	52
	$Mo(thd)_3$	H_2S	300	Si/SiO_2, Sods lime glass, ALD-SnS, Borosilicate glass, ITO-coated glass, etc.	P1	53
	BTBMMo	H_2S	250	Si/SiO_2, CNTs, Glass	P1	55
	$Mo(CO)_6$	CH_3SSCH_3	100	Si/SiO_2	P1	56
	$Mo(CO)_6$	H_2S	155−175	Si/SiO_2	P1	57
	$Mo(CO)_6$	HMDST	150	Al_2O_3	P1	58
	$Mo(CO)_6$	H_2S	175	Si/SiO_2	P1	59
	$MoCl_5$	H_2S	460	Si/SiO_2	P1	60
	$(NtBu)_2(NMe_2)_2Mo$	H_2S	150−450	Si/SiO_2	P2	76
	$MoCl_5$	H_2S	650	Si/SiO_2	P2	77
	$MoCl_5$	H_2S	400	Si/SiO_2, Al	P3	81
$MoSe_2$	$MoCl_5$	$(Me_3Si)_2Se$	300	Si/SiO_2, TiO_2, Glass	P1	69
WS_2	$C_{12}H_{30}N_4W$	H_2S	300	Si/SiO_2	P1	71
	WF_6	H_2S	300−450	Al_2O_3	P2	78
	$C_{12}H_{30}N_4W$	H_2S	400	Si/SiO_2, Al_2O_3	P3	73
WSe_2	WCl_5	H_2Se	390	Si/SiO_2	P1	75

[a]P1 indicates "The one-step ALD method for growing TMD films". P2 indicates "PE-ALD growth of TMD films". P3 indicates "ALD selective growth patterns".

and bottom-up approaches (chemical vapor deposition, sulfidation of metals or metal oxides, sputtering, physical vapor deposition, pulsed laser deposition, and ALD, etc.). Mechanical stripping methods lack scalability, leading to the appeal of chemical vapor deposition (CVD) due to its morphological control and scalability. Recent advancements have notably improved the quality of TMD layers produced through CVD. Moreover, ALD provides an alternative route for cultivating high-quality TMD films on a wafer-level, exhibiting substrate-wide uniformity and performance comparable to layers produced by conventional stripping methods. ALD, relying on surface saturation reactions, delivers self-limiting thin film deposition with atomic-level thickness control, uniformity, and large-area homogeneity. The capability of ALD to deposit superior films at lower temperatures positions it as the primary technique for fabricating nanoscale devices on diverse substrates or intricate 3D structures.

This review comprehensively examines recent advancements in the ALD growth of 2D TMDs. We provide an extensive overview of various 2D TMD layered materials, delving into the ALD processes for producing common TMDs such as MoS_2, WS_2, $MoSe_2$, and WSe_2. We evaluate potential growth mechanisms for ALD-prepared TMD materials, detailing their growth characteristics. The structural and physical properties of the TMD materials and the basic principles of ALD are first briefly discussed, followed by a detailed description of the ALD processes, growth characteristics of various TMD materials, and a list of practical applications of ALD-grown TMDs. Finally, we summarize current knowledge, explore ongoing research efforts, and provide an outlook on future directions.

2. THE ALD GROWTH STRATEGY AND PROCESSES FOR THE SYNTHESIS OF TMDS

ALD is a specially modified chemical vapor deposition method to grow thin films by self-limiting chemical reactions. ALD

https://doi.org/10.1021/acs.cgd.3c01044
Cryst. Growth Des. 2024, 24, 1865−1879

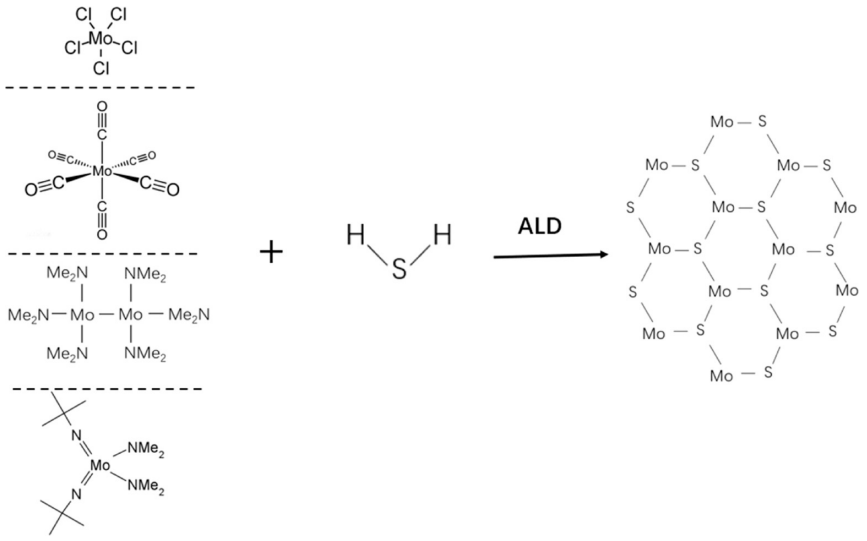

Figure 2. One-step ALD process for growing MoS_2 films.

involves the formation of thin films by pulsed alternating passes of gas-phase precursors into a reactor and chemisorbing and reacting on a substrate. Individual atomic layers are deposited by supplying inert gases (Ar, N_2, etc.) to separate the various reactants, and the thickness is controlled by repeated deposition. In other words, ALD is not deposited by a gas-phase reaction, but rather one reactant is adsorbed onto a substrate, and then a second or third gas enters and chemisorbs with the substrate to form a film. This reaction is called a self-limiting reaction. Self-limiting reactions occur only between the reactant and the surface, and the reactant and the reactant do not react, so they can be deposited in atomic layers. Parameters such as precursor molecules, pulse time, dose, growth temperature, substrate, and annealing conditions can be tuned during the ALD deposition process, as listed in Table 1. When depositing various TMD materials using ALD, different parameter combinations produce samples with different characteristics, leading to more research possibilities.

Three primary types categorize ALD precursors: inorganic, organometallic, and metal−organic.[14,15] Inorganic precursors lack carbon components, whereas metal−organic precursors incorporate organic ligands,[16] yet are devoid of metal−carbon bonds. On the other hand, organometallic precursors possess organic ligands with metal−carbon bonds. Traditionally, ALD metal precursors have been classified based on their ligands, such as halides, β-diketonates, alkyls, alkylamides, amidates, cyclopentadienes, guanidines, and more.[15,16] Recently, a new trend has emerged, utilizing heterosensory metal complexes that combine two or more distinct ligands to further tailor the precursor properties.[17−22] In ALD, metal halides, especially chlorides, find wide applications for depositing oxide- and sulfide-based 2D films.[23−27]

To develop a dependable formulation for each precursor, knowledge of the ALD process deposition temperature is crucial. ALD, being a surface-sensitive technique, requires a comprehensive recipe with detailed explanations for every setup procedure. Thus, the well-established ALD recipe for 2D nanomaterials is considered a highly valuable technical resource. The growth rate in ALD is contingent on the distinct chemical properties of the ALD surface[28] and is influenced by a diverse range of metal−organic precursors.[29,30] Moreover, the temperature range at which the ALD reaction concludes is termed the ALD window. The ALD process typically operates at much lower temperatures than CVD. Tailoring the growth rate during ALD deposition is more intricate than CVD, involving a delicate balance of precursor concentration, temperature, and purge time per pulse to maintain a stable growth rate per cycle (GPC).[18]

Careful selection of precursors is crucial since not all precursor combinations offer an ALD window. Moreover, the activation of the reaction at the designated temperature may sometimes require assistance beyond thermal energy, where UV light or plasma comes into play during the ALD process. The findings demonstrate that plasma-enhanced ALD (PE-ALD) enhances the growth rate by utilizing a greater number of precursors.

Evolved from its original concept, ALD now boasts expanded capabilities, allowing the growth of diverse inorganic materials like oxides,[31,32] nitrides,[33,34] sulfides, and more intricate compounds.[35] This surface-controlled process achieves atomic-level precision in thin film growth due to its unique mechanism, wherein a self-limiting surface reaction takes place on the substrate surface. Consequently, the thin films produced by ALD demonstrate remarkable uniformity, outstanding controllability, and are deposited at low temperatures. Our research focuses on reported ALD schemes for various TMDs materials, providing invaluable assistance for scientific investigations and industrial applications.

2.1. The One-Step ALD Method for Growing TMD Films. The ALD method initially used to prepare TMD films resulted in forming few-layer films. The process was improved using different precursors. Figure 2 shows the alternate deposition of transition-metal precursors with coreactants in a one-step method on the substrate inside the reaction chamber to obtain desired films directly. Further improvements to this method were made by using plasma, regioselective growth, and other approaches to improve the films' quality and the ALD method's applicability in device preparation.

The decomposition of a complete reaction in an ALD cycle into two half-reactions allows for breaking down the chemical reactions in chronological order. Surface-active sites must be fully depleted before halting one half-reaction, after which the other half-reaction commences. Figure 3 illustrates a schematic

https://doi.org/10.1021/acs.cgd.3c01044
Cryst. Growth Des. 2024, 24, 1865−1879

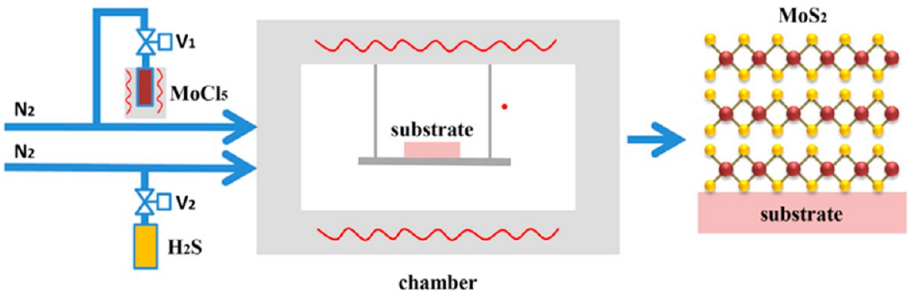

Figure 3. Schematic diagram of the ALD MoS_2 growth process.[36] Reprinted (adapted) with permission from ref 36. Copyright 2017 Elsevier.

diagram of MoS_2 preparation via ALD. A growth cycle involves four steps: exposing to $MoCl_5$, N_2 purging, exposing to H_2, and another N_2 purging. To achieve the desired thickness of the MoS_2 film, this sequence can be iterated. The ALD process facilitates chemical reactions on the new atomic layer, directly influenced by the preceding layer, enabling deposition of only one atomic layer per reaction. Owing to self-limiting reactions, precise regulation of the thickness of the film on an atomic scale and homogeneous coverage on structurally complicated substrates are achieved. Furthermore, ALD exhibits high reproducibility as it remains insensitive to excess precursors. Therefore, ALD represents a favorable method for preparing 2D TMD films.

2.1.1. MoS_2. Molybdenum disulfide (MoS_2), which is one of the 2D TMDs, has garnered significant attention owing to its remarkable semiconducting and optical characteristics.[37−41] The hexagonal network structure of MoS_2 consists of Mo and S atoms covalently bonded, providing exceptional stability. Additionally, weak interlayer bonding arises from vdW forces.[42,43] Consequently, MoS_2 exhibits a tunable bandgap structure dependent on layer number. For instance, the bandgap rises from approximately 1.2 eV (indirect) to around 1.8 eV (direct) when transitioning from bulk MoS_2 to monolayers.[44,45] The appealing on/off ratio and carrier mobility at room temperature make MoS_2 a promising candidate for electronic and optoelectronic applications.[42,46,47]

In a study by Tan et al.,[48] the ALD has been used for the growth of MoS_2 films ranging from monolayers to multilayers on a sapphire substrate with the use of $MoCl_5$ and H_2S as precursors at a growth temperature of 300 °C. The ALD process allowed accurate regulation of the MoS_2 film gauge as a result of the pulsed injection of reactants and the property of self-confined reaction of H_2S and $MoCl_5$. Subsequently, postdeposition annealing of the monolayers improved the films' crystallinity, as evidenced by the presence of triangular crystals with strong visible photoluminescence. Likewise, Liu et al.[49] managed to prepare single-molecule films with controlled layered structures and ultrathin MoS_2 films containing MoS_2 triangular crystals of specific thickness using ALD. They achieved highly oriented hexagonal crystal structures through certain ALD cycles. Furthermore, Browning et al.[50] utilized ALD to grow MoS_2 films on SiO_2-coated silicon wafers (5 cm × 5 cm area) employing $MoCl_5$ and H_2S as precursors. By regulating the experimental conditions, they successfully prepared smooth, uniform, and continuous films in the 350−450 °C temperature region, with a linear relationship observed between the growth of the film and the number of ALD cycles. Liu et al.[51] achieved uniformly deposited MoS_2 films at comparatively high growth rates by using $MoCl_5$ and hexamethyldisilicon sulfide (HMDST) as ALD precursors. They controlled the thickness on 50 mm sapphire and 100 mm silica substrates. The films were utilized to prepare large-scale top-gate FET arrays with a room-temperature migration rate of 0.56 $cm^2/(V·s)$ and a high on/off current ratio of 10^6. Across the sapphire wafer, superb electrical uniformity was observed. In addition, logic circuits, including inverters, AND, NOR, and OR gates, were successfully implemented through a high-k HfO_2 dielectric layer. Their inverters exhibited a rapid response frequency of 50 Hz at VDD = 4 V and a DC voltage gain of 4 V. These results indicate the method's potential for large-scale synthesis of high-quality MoS_2 films with low toxicity and high efficiency, enabling broader future applications.

Huang et al.[36] used a one-step ALD method without high-temperature annealing to prepare highly crystalline MoS_2 films. They employed $MoCl_5$ and H_2S as precursors and Si and sapphire as substrates. At different growth temperatures ranging from 420 to 480 °C, the grain size of the films could be adjusted from ∼20 to ∼100 nm, with excellent crystalline properties guaranteed between 430 and 470 °C. Due to the decomposition of functional groups, the growth temperature should not exceed 480 °C. And more, this work confirmed that Al_2O_3 is a more favorable substrate than Si (as depicted in Figure 4), resulting in thicker films on Al_2O_3 compared to Si substrates. This generates more necessary hydroxyl groups in the initial surface reactions. The mean growth rate of highly crystalline MoS_2 films is about 4.3 Å/cycle on Al_2O_3 substrates and approximately 3.8 Å/cycle on Si substrates. Raman spectroscopy, scanning electron microscopy (SEM), and transmission electron microscopy (TEM) (Figure 5) were

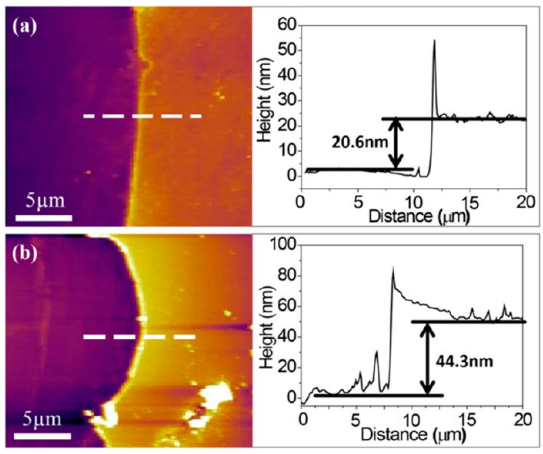

Figure 4. AFM images and height distribution of MoS_2 films obtained after 100 ALD cycles on (a) Si and (b) Al_2O_3 substrates.[36] Reprinted (adapted) with permission from ref 36. Copyright 2017 Elsevier.

https://doi.org/10.1021/acs.cgd.3c01044
Cryst. Growth Des. 2024, 24, 1865−1879

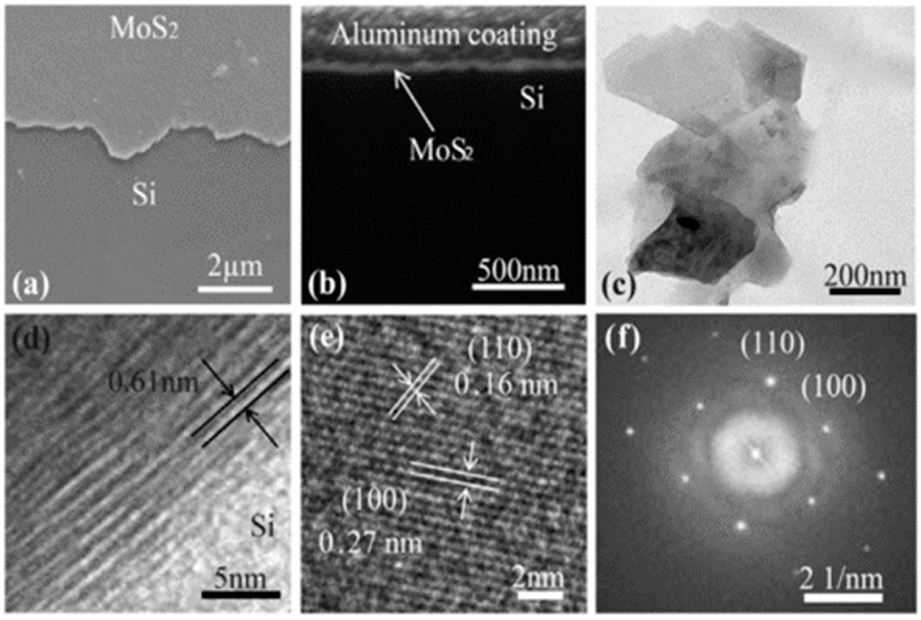

Figure 5. (a) SEM image of the 100-cycle ALD MoS_2 film on the Si substrate. (b) SEM image of the cross-section of (a). (c) TEM image of the MoS_2 film exfoliated from the Si substrate. (d) Cross-sectional TEM image of the MoS_2 film deposited on the Si substrate. (e) TEM image of the MoS_2 film showing a crystalline film. (f) Fourier transform election diffraction of (e).[36] Reprinted (adapted) with permission from ref 36. Copyright 2017 Elsevier.

used for the characterization of the resulting MoS_2 films, revealing their well-defined structure.

In addition, several researchers have used organic sources of molybdenum. For example, Jurca et al.[52] reported the ALD of MoS_2 below 60 °C using the tetrakis(dimethylamine)-molybdenum metal−organic precursor. Compared to halide precursors, metal−organic precursors enable the ALD growth of TMDs at low temperatures due to their high reactivity with oxidants. Low ALD growth temperatures are compatible with photolithography and stripping patterning to fabricate various device structures directly. The use of metal−organic precursors in the reaction prevents harmful effects from potential byproducts when halide precursors react with reactants, such as hydrochloric acid. Meanwhile, processes based on the less volatile organosulfur precursor, CH_3SSCH_3, compared to H_2S gas, might lead to the generation of sulfur contaminants harmful to reactor components and deposited films. Mattinen et al.[53] demonstrated the deposition of crystalline MoS_2 films using the molybdenum precursor $Mo(thd)_3$ and H_2S in an ALD process at 300 °C. ALD exhibited self-limiting growth and precise film thickness control, along with excellent film uniformity. In-depth characterization revealed details about film growth, morphology, crystallinity, composition, and optical properties on various substrates. However, significant differences were observed in film growth, morphology, and crystallinity on different substrates. Shirazi et al.[54] used density functional theory in an attempt to study the reaction of precursors on the surface of silica substrates in the ALD reaction, which was directed toward the growth of molybdenum disulfide with $Mo(NMe_2)_2(NtBu)_2$ and H_2S as precursors. The study reveals the reaction process from the initial physical adsorption of precursors on the substrate surface to the subsequent growth of molybdenum sulfide from the interaction of precursors on the substrate surface. First, protons on the hydroxyl groups on the exposed surface of silica on the substrate surface were transferred to the physisorbed molybdenum precursor $Mo(NMe_2)_2(NtBu)_2$, which increased the Lewis acidicity of molybdenum and the Lewis basicity of oxygen, and then the chemisorption of molybdenum precursor on the surface was achieved. According to the findings, the transfer of protons from the silica surface to the dicarboxamide ligand favors the formation and desorption of dimethylamine to the detriment of *tert*-butylamine, and the cooperation between hydrogen sulfide molecules (the "cooperation" mechanism) also greatly affects the formation of *tert*-butylamine, which is one of the two-dimensional molybdenum disulfides for the initial ALD on silica substrates critical step. Cyclic ALD reactions resulted in the formation of buffer layers, which could affect the electrical and optical properties of subsequently deposited 2D layers. Shen et al.[55] introduced a low-temperature ALD system using bis(*tert*-butylimino)bis-(dimethylamino)molybdenum(VI) (BTBMMo) and H_2S as molybdenum precursors and sulfur sources, respectively, at temperatures below 250 °C. They successfully deposited MoS_2 on silicon wafers, carbon nanotubes (CNTs), and glass, achieving various morphologies like smooth films, vertical nanosheets, and nanodots, controlled by various conditional parameters for ALD. The quality of the final molybdenum disulfide (MoS_2) films was systematically investigated concerning annealing temperature and environment, affecting optical properties and electrocatalytic activity. Vertically grown MoS_2 thin films outperformed smoothly deposited ones due to their higher surface area and concentration of catalytically active surface centers. The advantages of this low-temperature ALD process for growing morphology-controlled MoS_2 thin films make it promising for electronic, catalytic, and sensing devices.

Jin et al.[56] presented a novel ALD approach for molybdenum disulfide growth on SiO_2/Si substrates at 100 °C. Molybdenum hexacarbonyl ($Mo(CO)_6$) and dimethyl disulfide (CH_3SSCH_3, DMDS) were used as molybdenum and sulfur precursors, respectively. The annealing process at 900

https://doi.org/10.1021/acs.cgd.3c01044
Cryst. Growth Des. 2024, 24, 1865−1879

°C for 5 min under argon led to the crystallization of MoS_2, aligning it parallel to the substrate. The resulting amorphous MoS_2 can serve catalytic applications like the hydrogen precipitation reaction (HER), while crystallized MoS_2 from annealing is suitable for electronic applications. Similarly, Pyeon et al.[57] reported ALD of MoS_2 films utilizing $Mo(CO)_6$ and H_2S as molybdenum and sulfur precursors. The ALD window was limited to 155−175 °C for self-limited growth. Longer H_2S exposure was necessary to reduce impurity content in the films. Lower growth temperatures resulted in amorphous MoS_2 films, but postannealing at high temperatures under an hydrogen sulfide atmosphere improved crystal quality of MoS_2 films. Remarkably uniform film growth was achieved even on 4-in SiO_2/Si wafers. Zhang et al.[58] synthesized large MoS_2 films with controlled thickness on sapphire substrates at 150 °C via ALD, using $Mo(CO)_6$ and hexamethyldisilicate (HMDST) as precursors. High-temperature annealing in a sulfur atmosphere removed ALD-MoO_3 from the MoS_2 films. The introduction of HMDST enabled a nontoxic process, avoiding harmful sulfur precursors like CH_3SSCH_3 and H_2S. The ALD MoS_2 films exhibited desirable properties such as high uniformity, wafer-level thickness uniformity, reproducibility, and thickness controllability, enabling the fabrication of field-effect transistor (FET) arrays with excellent electrical properties. Kim et al.[59] introduced a new ALD program for uniform growth of monolayer MoS_2 films on a wafer scale. The process used H_2S and $Mo(CO)_6$ at 175 °C. By adjusting the precursor injection step to divide the feeding process, precise control over the precursor adsorption in each cycle beyond the typical ALD reaction was achieved. As a result, a complete monolayer MoS_2 film was successfully prepared in a single ALD cycle.

Yang et al.[60] proposed a possible approach for obtaining 2D molybdenum disulfide with increased particle size through drop-flow ALD on nickel foam (as shown in Figure 6). MoS_2

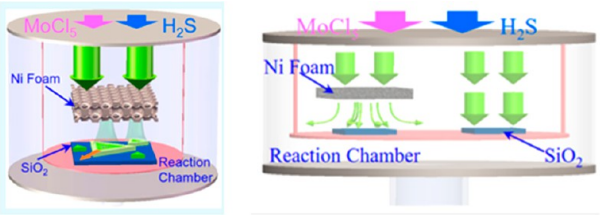

Figure 6. Schematic diagram of the drop flow ALD.[60] Reprinted (adapted) with permission from ref 60. Copyright 2019 American Chemical Society.

grains with sizes exceeding 420 nm (single-layer samples) and exceeding 400 nm (five-layer samples) were achieved at 460 °C, using a 1 mm-thick nickel foam coverage with a 2 mm gap from the substrate. The use of nickel foam reduced nucleation density by transforming the precursor flow into a drop-flow-fluidized source flow, resulting in increased grain size during parallel growth around the nuclei, considering spatial site resistance. Additionally, the nickel foam enhanced heat transfer around the substrate, leading to obtained higher crystallinity. This work opens up attractive opportunities for high-quality two-dimensional materials with wafer-level uniformity in applications.

2.1.2. $MoSe_2$. $MoSe_2$ are attractive in photonics and optoelectronics due to their bandgap energy in the UV−visible region.[61,62] In the realm of renewable solar energy research, $MoSe_2$ has been employed as a catalyst for the HER.[63,64] Additionally, both $MoSe_2$ and MoS_2 serve as excellent photoelectrodes in electrochemical regenerative solar cells due to their reduced susceptibility to photolysis. Furthermore, recent studies have highlighted the promise of $MoSe_2$ as an alternative electrode for sodium-ion and lithium-ion batteries as well as supercapacitors due to the larger distance between the layers (0.65 nm). Moreover, $MoSe_2$ has been investigated for various other applications, including its potential as a sensor, photodetector, electrocatalyst, and photocatalyst. This is attributed to its narrow bandgap (1.33−1.72 eV), high resistance to photocorrosion, and the electrochemically active unsaturated selenium edge.[65−68] Nevertheless, the availability of volatile organoselenium compounds suitable for ALD has been limited. To address this, Charvot et al.[69] expanded the portfolio by scheming and synthesizing a range of tetra-, penta-, and hexameric cyclic silicaselenides. The properties of these compounds are influenced by the cyclic silicaselenide size and the amount of flush bonding Se atoms, together with alternating alkyl chains on the periphery. Unlike previous methods involving sodium or lithium selenide production, the new synthesis approach involves a direct reaction of monomeric selenium containing chlorosilane. Notably, the new type 2,2,4,4-tetraisopropyl-1,3,2,4-dienodiethane demonstrated excellent chemical/thermal stability and reactivity, facilitating a successful gas−solid phase reaction with $MoCl_5$ to produce high-purity $MoSe_2$. Comprehensive characterization of the 2D $MoSe_2$ sheet in the deposited state revealed its out-of-plane orientation. As a result, the developed quaternary cyclic selenide serves as an ideal selenium precursor for $MoSe_2$ ALD, offering promising prospects for further research and practical applications.

Zazpe et al.[70] achieved successful growth of glass substrate with $MoSe_2$ nanoflakes using ALD, employing $MoCl_5$ and $(Me_3Si)_2Se$ as precursors. In this study, they expanded the scope by synthesizing and investigating a broader range of novel alkyl tin $(R_3Sn)_2Se$ and alkyl $(R_3Si)_2Se$ compounds for ALD-based $MoSe_2$ nanosheet growth, utilizing various Mo precursors. Thorough assessments were conducted on the combination of these selenium compounds with different molybdenum precursors to identify dependable selenium precursors. The composition and morphology of the deposited materials on TiO_2 surfaces (with the use of annealed titanium foil), glass, and silicon wafers were analyzed by scanning electron microscopy (as shown in Figure 7). The characterization confirmed the growth of polycrystalline multilayer $MoSe_2$ nanosheets with out-of-plane orientation on various substrates. To investigate the evolution of the growth of $MoSe_2$ during the early stages of ALD, high-resolution transmission electron microscopy has been used. The results indicated 2H-hexagonal molybdenum diselenide nanosheets island growth mode, initially adopting both in-plane and out-of-plane orientations. However, with an increasing number of ALD cycles, the dominant orientation of the $MoSe_2$ nanosheets shifted to a random orientation out of the plane, as shown in the AFM results (as shown in Figure 8).

In conventional ALD for thin films, a gas-phase surface confinement reaction is employed, whereas electrochemical atomic layer deposition (E-ALD) relies on an electrochemical surface confinement reaction. Tsang et al.[71] conducted a successful growth of $MoSe_2$ utilizing E-ALD. The electrochemical surface confinement reaction is commonly known as underpotential deposition (UPD). In the E-ALD process,

https://doi.org/10.1021/acs.cgd.3c01044
Cryst. Growth Des. 2024, 24, 1865−1879

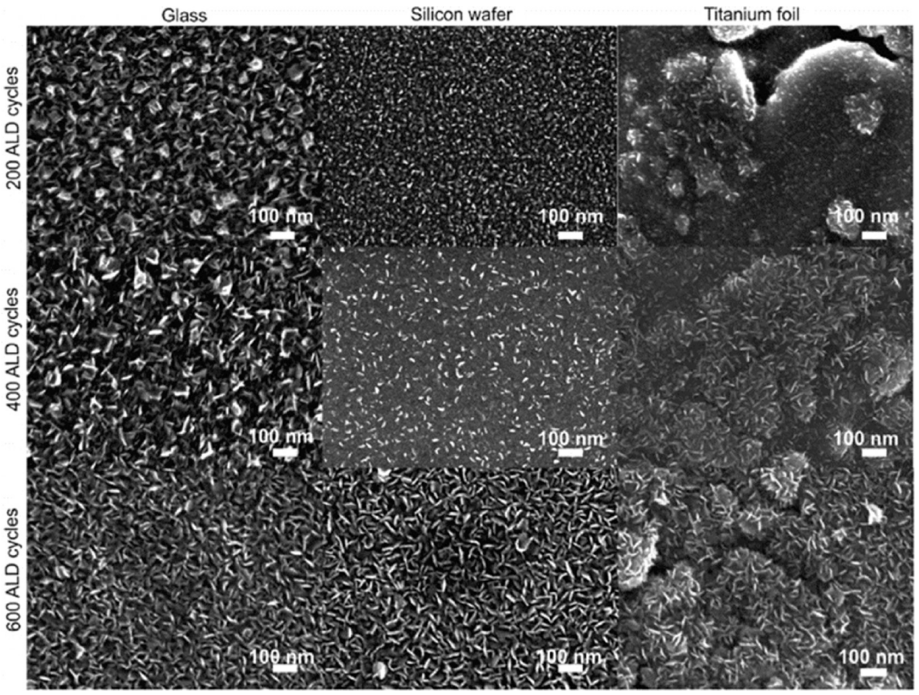

Figure 7. SEM top-view images of $MoSe_2$ nanosheets grown using $(Me_3Si)_2Se$ as the Se precursor and $MoCl_5$ as the Mo precursor on different substrates (glass, Si wafer, and thin anatase TiO_2) upon applying different number of ALD cycles: 200, 400, and 600.[70] Reproduced with permission under CC BY-NC-ND 4.0 from ref 70. Copyright 2020 Elsevier.

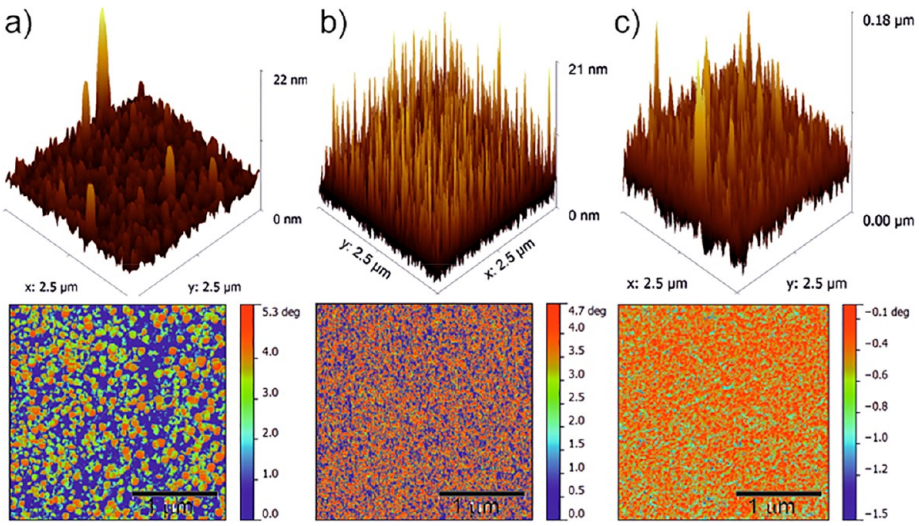

Figure 8. Three-dimensional morphology (top) and phase comparison (bottom) of $MoSe_2$ deposited on Si wafers during (a) 200, (b) 400, and (c) 600 $MoSe_2$ ALD cycles with $MoCl_5$ as the Mo precursor and $(Me_3Si)_2Se$ as the Se precursor.[70] Reproduced with permission under CC BY-NC-ND 4.0 from ref 70. Copyright 2020 Elsevier.

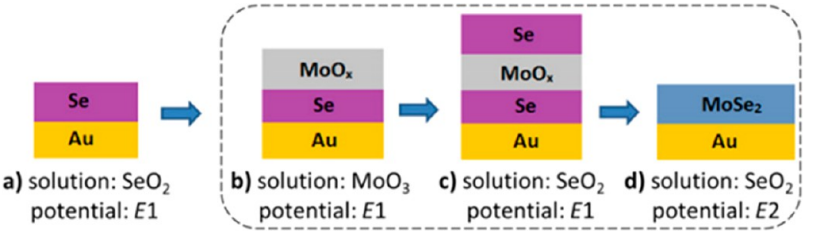

Figure 9. A simplified scheme for forming $MoSe_2$ by E-ALD. Se UPD on Au is performed at the beginning of a deposition (step a). Steps b to d are iterated to deposit $MoSe_2$ in an ALD manner.[71] Reproduced with permission from ref 71. Copyright 2017 Elsevier.

https://doi.org/10.1021/acs.cgd.3c01044
Cryst. Growth Des. 2024, 24, 1865−1879

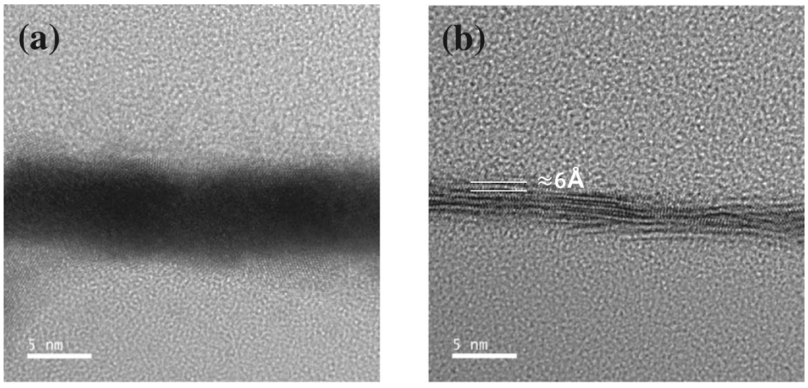

Figure 10. High-resolution XTEM images of (a) as-grown and (b) annealed WS_2 films revealing the amorphous and layered structure of the films, respectively.[74] Reproduced with permission from ref 74. Copyright 2021 IOP Publishing.

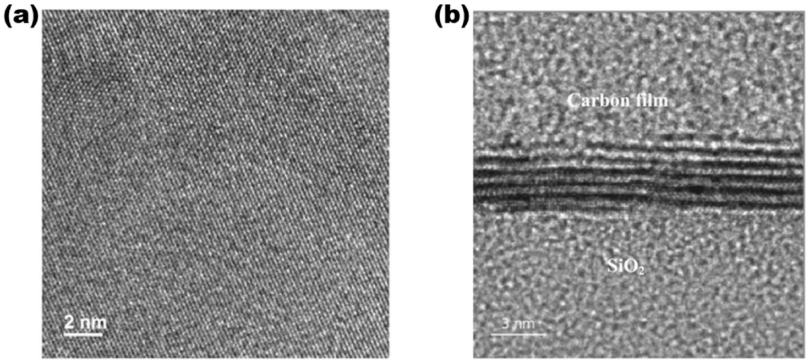

Figure 11. (a) Top-view TEM scan of WSe_2; (b) cross-sectional TEM image of a multilayer thick WSe_2 film.[76] Reproduced with permission from ref 76. Copyright 2016 IOP Publishing.

desired components are alternately deposited in cycles to determine the thickness of the deposition. To prepare $MoSe_2$ films, Au wafers' voltammetric behavior in SeO_2 and MoO_3 solutions was examined under acidic and alkaline conditions. Acidic precursor solutions, 0.5 mM SeO_2, and 1 mM $HMoO_4^-$ adjusted to pH 1.5, were used for the $MoSe_2$ deposition through E-ALD. Figure 9 illustrates the simplified E-ALD cycling scheme applied to generate $MoSe_2$ films successfully. Tests revealed the existence of molybdenum diselenide and found that there was also molybdenum dioxide in the films that did not participate in the reaction. Subsequent thermal annealing effectively eliminated MoO_2 and improved the film crystallinity, although they remained XRD amorphous. Throughout the $MoSe_2$ Raman peaks' temperature variation analysis, it was evident that annealing contributed to the enhancement of film crystallinity. However, the films still maintained their XRD amorphous nature.

2.1.3. WS_2. WS_2 has a similar structure to MoS_2 and can be potentially applied in chemical sensors, lithium-ion batteries, transistors, etc. Wu et al.[72] presented a WS_2 ALD process based on bis(*tert*-butylamino)bis(dimethylamino)tungsten-(VI), and hydrogen sulfide as a source of sulfur. Based on the study of the reaction of tungsten precursors with silica, the self-limiting properties of the process were determined, a wide range of reaction parameters, including the temperature of reaction chamber, precursor temperature, and duration of each ALD step, was optimized, and a possible reaction mechanism was proposed. Yang et al.[73] carried out a systematic research of the synthesis of WS_2 using ALD. The results showed that the synthesis of various morphologies of ALD-WS_2 could be precisely controlled. The nucleation density greatly influences the nucleation and growth mechanisms of WS_2. An abrupt increase in the nucleation density after continuous film formation leads to a change of growth mechanism from lateral film growth to vertical nanowire growth. The lateral and vertical growth mechanisms coexist and compete with each other at different growth stages. The top gate FETs based on the prepared WS_2 films showed a high switching ratio of 10^5 and a field-effect carrier mobility of 3.21 $cm^2/(V\ s)$. Kim et al.[74] used a metal−organic precursor $W(CO)(CH_3CH_2C{\equiv}CCH_2CH_3)_3$ and H_2S at a comparatively low temperature of 300 °C to perform the ALD of WS_2 on several types of substrates. By varying the precursors and reactants, typical self-limited film growth was achieved with cycle growth values of approximately 0.13 nm, as depicted in Figure 10. Although the grown films were amorphous, XTEM analysis suggested the possibility of obtaining crystalline WS_2 films through annealing in an H_2S atmosphere at temperatures exceeding 700 °C. Scharf et al.[75] detailed the synthesis, structure, and tribological properties of ALD-grown nanocomposite WS_2 solid lubrication films. They established a new catalytic pathway involving the diethylzinc catalyst to facilitate WS_2 adsorption and growth. Thin films up to 8 nm thick were grown on Si, SiO_2, stainless steel, polycrystalline Si, and plated Ni microelectromechanical system structures by continuous exposure to WF_6 and H_2S gas. The use of zinc-catalyzed WF_6 adsorption and reaction significantly enhanced the WS_2 growth rate. Furthermore, the hexagonal crystal structure of ALD WS_2 was found to be temperature-dependent.

https://doi.org/10.1021/acs.cgd.3c01044
Cryst. Growth Des. 2024, 24, 1865−1879

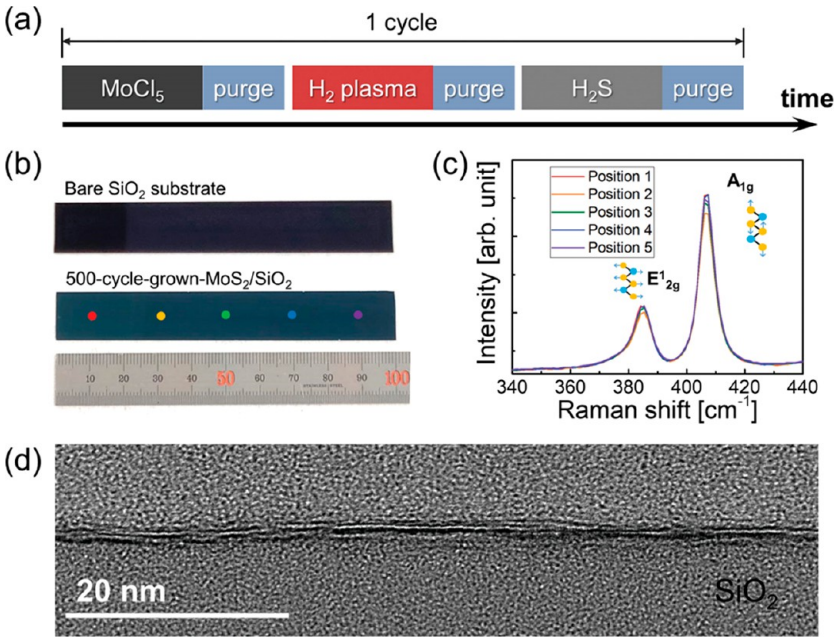

Figure 12. (a) Schematic of the ALD sequence for synthesizing MoS_2 layers. (b) Photograph of a bare SiO_2 (285 nm)/Si substrate and 500-cycle-ALD-grown MoS_2/SiO_2 (285 nm)/Si. (c) Raman spectra of the MoS_2 obtained at positions indicated in b. (d) HRTEM image of 500-cycle-ALD-grown $MoS_2/SiO_2/Si$.[78] Reproduced with permission from ref 78. Copyright 2022 Royal Society of Chemistry.

2.1.4. WSe_2. Browning et al.[76] used ALD to grow smooth and continuous WSe_2 films on the surface of a 5 cm × 5 cm substrate consisting of a Si wafer and a SiO_2 layer, with WCl_5 and H_2Se as ALD precursors and a growth temperature of 390 °C. As shown in Figure 11, the properties of the films characterized by TEM were comparable to those of WSe_2 films prepared by chemical vapor deposition and exfoliation.

2.2. PE-ALD Growth of TMD Films. Extensive research efforts have been dedicated to addressing the limitations of conventional ALD, with a focus on enhancing film size and quality. One common improvement involves incorporating plasma gas into the reaction. For instance, Sharma et al.[77] employed plasma-enhanced atomic layer deposition (PE-ALD) to synthesize tunable morphologies of MoS_2, ranging from monolayers to multilayers, at low temperatures. The process utilized $[(NtBu)_2(NMe_2)_2Mo]$ as the molybdenum precursor, and coreactants Ar + H_2 + H_2S (40 sccm argon; 8 sccm hydrogen; 2 sccm hydrogen sulfide plasma gas mixture from inductively coupled plasma source) on a SiO_2/Si substrate. Precise control over monolayer thickness and adjustable morphology were achieved by variation of the deposition temperature from 150 to 450 °C. Through detailed TEM studies, it was hypothesized that improved precursor sorption on high-energy edge sites of molybdenum disulfide during ALD growth contributed to the conversion to out-of-plane oriented films at 450 °C. Interestingly, for electrocatalysis using the HER, out-of-plane oriented films exhibited better performance than in-plane oriented ones.

Cho et al.[78] also synthesized MoS_2 using ALD, incorporating additional injection of remote H_2 plasma at a higher growth temperature of 650 °C to promote the surface migration of adsorbed atoms. The use of inorganic precursors such as molybdenum(V) chloride ($MoCl_5$) with a high decomposition temperature enabled the achievement of such elevated growth temperatures. Introduction of remote H_2 plasma further reduced impurities, like oxygen and chlorine, in the films. Activated species grown at high temperatures facilitated easy surface diffusion of adsorbates, resulting in improved crystallinity, characterized by fewer structural defects and larger particle size. The injection of H_2 plasma generated separately from the reactor, which flows into the reactor, facilitated the reduction of Mo ions from a +5 oxidation state in $MoCl_5$ to a +4 oxidation state in MoS_2 during the ALD process (as shown in Figure 12a). The use of a remote plasma system reduced plasma damage to the film surface, yielding a high-quality MoS_2 film. Figure 12b displayed MoS_2 layers with excellent thickness uniformity, evident from the invariable distance between the E^1_{2g} and A_{1g} Raman peaks at different locations on the wafer (Figure 12c) with good crystallization. Additionally, Figure 12d depicted a cross-sectional high-resolution transmission electron microscopy (HRTEM) image of MoS_2 grown on SiO_2, where the layer structure and the well-developed basal (002) plane parallel to the substrate surface were clearly observed.

The effect of reducing agents on ALD of tungsten hexafluoride and hydrogen sulfide precursor tungsten disulfide was demonstrated by Delabie et al.[79] They obtained nanocrystalline WS_2 layers with 2D structures using WF_6 and H_2S as precursors and passing H_2 plasma. These layers were deposited at low temperatures (300−450 °C) on Al_2O_3 substrates without templates or annealing. The component of the growth products largely depended on the H_2 plasma power and exposure time. Mild H_2 plasma conditions were necessary to achieve an S/W ratio of 2 for WS_2 layers. Groven et al.[80] proposed a qualitative model for the nucleation behavior of WS_2 on dielectric surfaces during PE-ALD processes. They utilized tungsten hexafluoride (WF_6), hydrogen (H_2) plasma, and hydrogen sulfide (H_2S) for their analysis of WS_2 crystal morphology. The study demonstrated that PE-ALD promoted lateral growth based on nucleation behavior insights. This understanding of the nucleation mechanism may be extended to other atomic layer deposition procedures for two-dimensional materials, allowing structure and property tuning at low deposition temperatures. Moreover, selective lateral growth of

https://doi.org/10.1021/acs.cgd.3c01044
Cryst. Growth Des. 2024, 24, 1865−1879

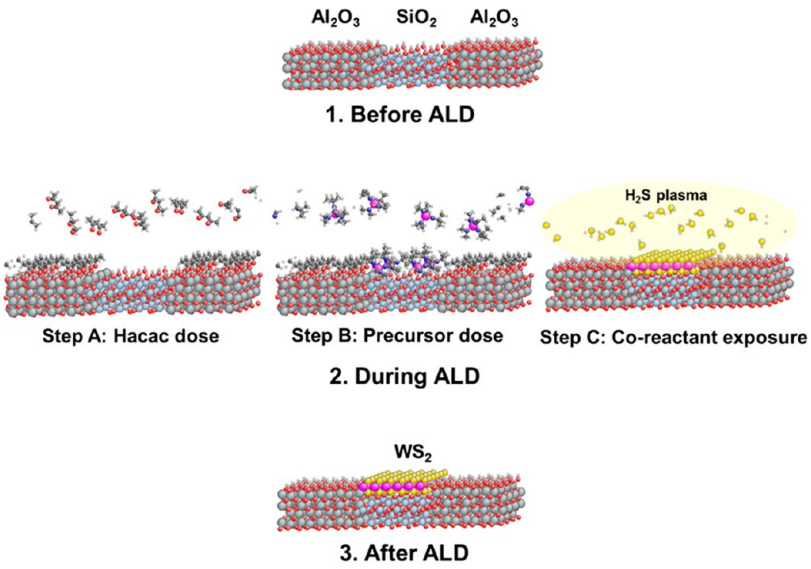

Figure 13. A schematic illustration of the area-selective ALD process for WS_2 is presented, utilizing ABC-type ALD cycles. Shown are the patterned surfaces of Al_2O_3/SiO_2 before, during, and after ALD. The specific ALD steps of the ABC-type cycle are as follows: Step A involves the dose of Hacac, Step B utilizes the tungsten precursor, bis(*tert*-butylimido)-bis(dimethylamido), and Step C exposes the surface to H_2S plasma. Through this method, WS_2 is selectively deposited on SiO_2 in the presence of Al_2O_3.[82] Reproduced with permission from ref 82. Copyright 2017 American Chemical Society.

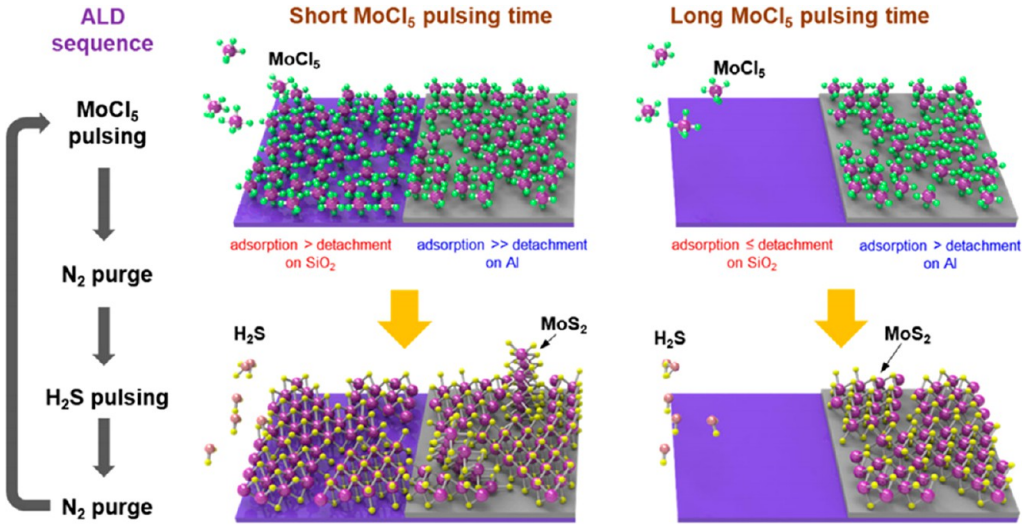

Figure 14. Illustration of the area-selective process of MoS_2 using $MoCl_5$ and H_2S precursors on different surfaces, namely SiO_2 and Al.[83] Reproduced with permission from ref 83. Copyright 2021 John Wiley and Sons.

single-crystal WS_2 from reaction seeds during the PE-ALD process facilitated 2D material growth at predetermined locations while keeping grain boundaries outside the active region.

Yeo[81] employed hydrogen sulfide plasma and tungsten hexacarbonyl for PE-ALD to grow WS_2 films on various substrates at a comparatively low temperature of 350 °C. The approach produced polycrystalline tungsten disulfide films with the preferred (002) growth, achieving high-quality films after 30 ALD cycles. Density functional theory (DFT) calculations revealed that H_2S plasma enhanced $W(CO)_6$ adsorption and CO ligand removal by creating different defect locations on the substrate. Analytical characterization of WS_2 films grown on Si/SiO_2 substrates confirmed high purity and well-defined stoichiometric ratios of the polycrystalline films. The deposited WS_2 films were utilized as electrodes in energy generation and storage applications. Uniform and conformal growth on a 3D nickel foam with a high specific surface area resulted in excellent hydrogen evolution reaction catalysis. Furthermore, the films grown on stainless steel substrates displayed stable electrochemical performance with a high area capacity after 50 charge/discharge cycles.

2.3. ALD Selective Growth Patterns. Selective deposition of TMD thin films using ALD has gained significant interest, and two methods for achieving this are discussed. Balasubramanyam et al.[82] were the pioneers in combining two pivotal pathways for atomic-level processing, namely, area-selective atomic layer deposition (AS-ALD) and the growth of two-dimensional materials. In their groundbreaking work, they demonstrated the bottom-up processing of 2D WS_2 nanospheres. To achieve this, they employed the AS-ALD method, as depicted in Figure 13, which involved prefabricating Al_2O_3

https://doi.org/10.1021/acs.cgd.3c01044
Cryst. Growth Des. 2024, 24, 1865−1879

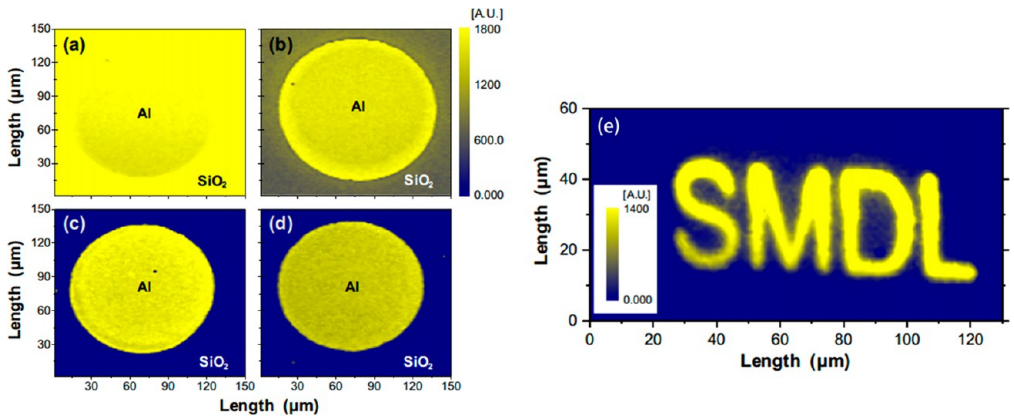

Figure 15. (a–d) Raman mapping images (A1g peak intensity) of the circular Al pattern that underwent the MoS_2 ALD process with $MoCl_5$ pulsing times of 1 s (a), 2 s (b), 3.5 s (c), and 5 s (d). (e) Raman mapping image (A_{1g} peak intensity) of the letter Al pattern after the MoS_2 ALD process for 100 cycles with a $MoCl_5$ pulsing time of 5 s at 400 °C. Reproduced with permission from ref 83. Copyright 2021 John Wiley and Sons.

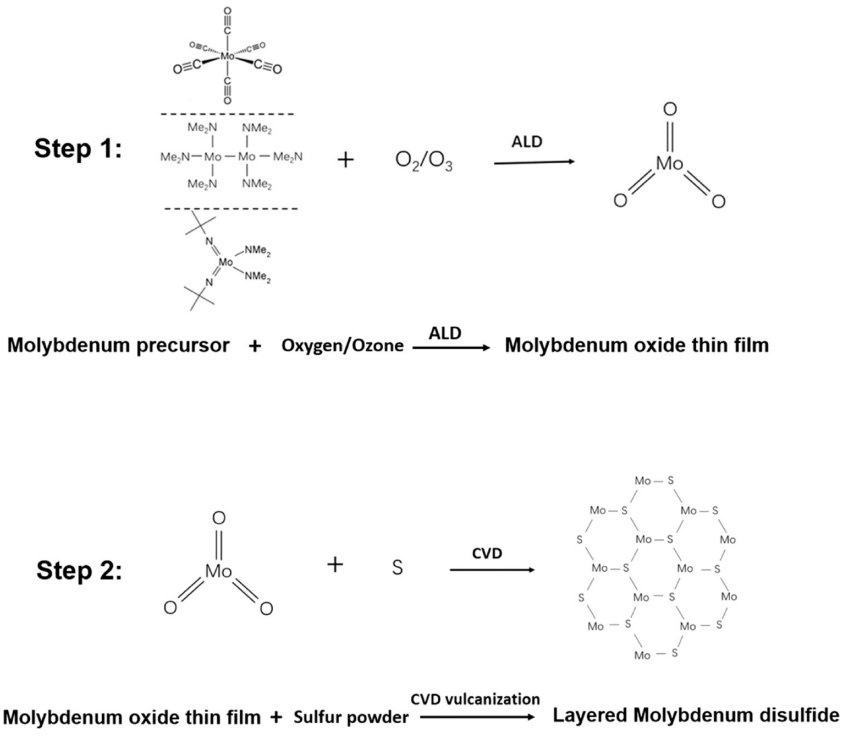

Figure 16. Diagram of a two-step ALD process with MoS_2 as an example.

(nongrowing region) and SiO_2 (growing region) surfaces using a three-step (ABC-type) ALD process. The selective deposition of WS_2 nanospheres was accomplished through an ABC-type plasma-enhanced ALD process at a low deposition temperature of 250 °C, wherein acetylacetone served as an inhibitor (A), bis(*tert*-butylimino)-bis-(dicarboxamide)-tungsten as a precursor (B), and H_2S plasma as a coreactant (C). The ingenious AS-ALD process facilitated rapid WS_2 growth on SiO_2 while effectively inhibiting growth on Al_2O_3. This technique also allows for selective growth on various transition-metal oxides and transition metal dichalcogenides (TMDs). Moreover, the promising outcomes of this study are expected to lay the groundwork for the regioselective ALD of other 2D materials.

An innovative approach proposed by Anh et al.[83] employs $MoCl_5$ and H_2S precursors for selective ALD of MoS_2. The mechanism for regioselective deposition is illustrated in Figure 14. During the initial ALD cycle, injecting $MoCl_5$ precursor vapor briefly leads to surface adsorption outweighing the self-etching effect ($MoCl_x$ stripping), causing MoS_2 growth on SiO_2 and Al surfaces. However, $MoCl_5$ adsorption on Al surpasses that on SiO_2, resulting in vertical MoS_2 crystal growth on Al due to increased deposition rates. Extending the $MoCl_5$ precursor exposure time enhances $MoCl_x$* shedding and self-etching effects on the SiO_2 surface, owing to weaker binding energy. Although Al still exhibits a higher deposition rate than SiO_2, self-etching becomes more favorable, leading to successful selective deposition. This approach capitalizes on $MoCl_5$'s simultaneous deposition and etching properties for regioselective MoS_2 ALD. By prolonging the $MoCl_5$ vapor introduction on SiO_2 surfaces, rapid suppression of MoS_2 growth occurs due to $MoCl_5$'s strong self-etching effect, separating weakly bound surface adsorbates ($MoCl_x$*). In contrast, the affinity of the aluminum surface for $MoCl_5$ offsets

https://doi.org/10.1021/acs.cgd.3c01044
Cryst. Growth Des. 2024, 24, 1865–1879

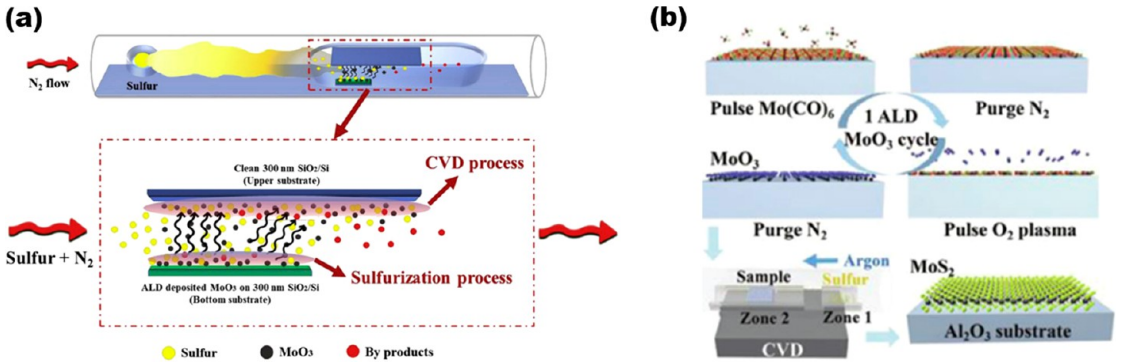

Figure 17. (a) Schematic diagram of the growth structure with simultaneous CVD/sulfidization.[84] Reproduced with permission from ref 84. Copyright 2020 Elsevier. (b) The ALD growth of MoO_3 films on the Al_2O_3 substrate, i.e., subsequent vulcanization to produce MoS_2 films.[86] Reproduced with permission from ref 86. Copyright 2017 John Wiley and Sons.

for the reduction of growth rate, enabling self-limited MoS_2 growth on SiO_2 substrates with prefabricated Al (5 nm) design (circular and letter patterns) (Figure 15), achieved through optimal $MoCl_5$ pulse timing.

2.4. The Two-Step ALD Method for Growing TMD Films. As shown in Figure 16, the two-step method refers to generating transition-metal oxide films using the ALD method followed by sulfidation of the transition-metal oxides with sulfur powder via a CVD tube furnace to finally obtain transition-metal sulfide compounds. In terms of layer controllability, the thickness of the TMD layer can be easily contained from single to multiple layers by controlling the thickness of the metal oxide before sulfidation. Demirtas et al.[84] used ALD-grown MoO_3 films as Mo precursors and grew uniform MoS_2 structures on top of the substrate by a CVD/sulfidation process in a subsequent step with good layer and size control. As shown in Figure 17a, the molybdenum disulfide growth occurred on two different substrates, clean SiO_2/Si (upper substrate) and ALD-deposited MoO_3 (lower substrate), placed face-to-face in a tube furnace at 690 °C, with simultaneous CVD/sulfidation reactions on the upper and lower substrates. The CVD process occurred on the upper substrate, while the sulfidation process occurred on the lower substrate. ALD MoO_3 provides two key advantages in the CVD/vulcanization of MoS_2, namely, uniform sublimation and control of the amount of Mo precursor vapor. The uniform sublimation of MoO_3 films provides uniform Mo vapor, allowing the repeated growth of MoS_2 across the substrate, and the amount of Mo precursors, and thus the size and layers, may be contained by varying the number of cycles in the ALD procedure. Keller et al.[85] improved the process of growing thin films of two-dimensional materials using ALD; they studied the initial nucleation characteristics of molybdenum oxide, and used the organic molybdenum precursor $(t\mathrm{BuN})_2(\mathrm{NMe}_2)_2\mathrm{Mo}$ and ozone to sulfide molybdenum oxide grown by conventional ALD and molybdenum oxide grown by plasma-enhanced ALD using the same molybdenum precursor as well as distal O_2 plasma, and finally successfully grew molybdenum disulfide thin films. Moreover, they explored the effect on the nucleation growth of molybdenum disulfide after sulfidation by adjusting various process parameters during the material growth process and treating the surface of molybdenum oxide, and then continuously optimized the process to obtain large-area homogeneous molybdenum disulfide thin films. Besides the insight into the oxide deposition control, film chemistry analysis was performed on several temperature profiles in a multistep sulfur-based process, which is less toxic than H_2S, detecting molybdenum reduction and sulfur doping achieved at relatively low temperatures by sulfiding ALD MoO_3 films deposited by ALD with molybdenum hexacarbonyl and oxidation as precursors, on sapphire substrates.[86] Growing molybdenum disulfide (MoS_2), the synthesized MoS_2 films have good layer controllability and uniformity, and molybdenum disulfide thin films with the required layer thickness may be achieved by changing the atomic layer deposition of the molybdenum oxide (MoO_3-ALD) cycle, as in Figure 17b.

Dai and colleagues[87] successfully synthesized wafer-scale nanosheets of molybdenum diselenide ($MoSe_2$) using a two-step method. Initially, they prepared molybdenum oxide (MoO_3) films through ALD and then subjugated them to selenization within a CVD tube furnace. By adjusting the ALD cycle during MoO_3 layer preparation, they achieved $MoSe_2$ nanosheets with the desired thickness. The synthesized $MoSe_2$ films demonstrated excellent control over layers, uniformity, and homogeneity at the wafer level. Raman and transmission electron microscopy (TEM) measurements confirmed that the $MoSe_2$ possessed a polycrystalline crystal structure with several layers. Additionally, photodetector arrays based on $MoSe_2$ were fabricated in various sizes, and their photoresponse was thoroughly investigated. These devices exhibited a rapid photoresponse time of 50 ms, a high switching ratio, and impressive photoresponsivity. Notably, the effective illumination area emerged as a critical application-related factor.

Song et al.[88] proposed a systematic layer-controllable synthesis process for WS_2 nanosheets on SiO_2 substrates using sulfated ALD WO_3 films, ensuring wafer-level homogeneity. The ALD-based WS_2 nanosheets exhibited good stoichiometric ratios, distinct Raman shifts, and bandgap dependence on the number of layers, as confirmed by X-ray photoelectron spectroscopy, Raman, and photoluminescence measurements. To evaluate the electrical properties of the monolayer WS_2 nanosheets, top-gate FETs were fabricated and characterized with high-k dielectric gate insulators. The synthesized WS_2 showed significantly higher field-effect electron mobility and lower subthreshold swing (SS) compared to previous reports. Additionally, exploiting the high conformality of the atomic layer deposition technology procedure, a technique for fabricating tungsten disulfide nanotubes was developed. Romanov et al.[89] introduced an indirect WS_2 synthesis method by seeding WO_3 films for sulfidation with ALD. This approach, governed by the concept

https://doi.org/10.1021/acs.cgd.3c01044
Cryst. Growth Des. 2024, 24, 1865−1879

of chemical saturation, ensured perfect reproducibility, uniform wafer size, and consistent 3D structures. The ALD-seeded WO_3 films exhibited distinct microstructures and impurity content compared to films obtained through other methods. In this study, the influence of the thickness of ALD-grown WO_3 seeded films on the structural and electrical properties of WS_2 films was investigated. The chosen method for preparing WS_2 films involved a sulfidation technique with preliminary WO_3 hydrogen reduction. Prior research has demonstrated the preparation of continuous WS_2 films with thicknesses down to three layers, limited by the selected ALD process.

SUMMARY AND OUTLOOK

ALD has proven successful in preparing TMD materials with precise thickness control, uniformity, and consistency on diverse substrates. These structures find extensive application in devices such as transistors, sensors, batteries, and catalysts. Postannealing is often significant to achieve improved crystallinity. However, some TMD materials remain undeveloped for ALD growth due to the need for enhanced film quality and suitable precursors. ALD offers the advantage of synthesizing high-quality TMD thin films at lower reaction temperatures, making it highly beneficial for certain applications. In conclusion, atomic layer techniques effectively fabricate controlled thickness TMD materials, despite crystallinity and nucleation challenges. As the demand for 2D materials rises, ALD is expected to gain significance in the field. Progress in ALD relies on precursor development and alternative chemistries to enhance film quality and manage surface reactivity. Particularly, challenges concerning thin film nucleation, adhesion, and impurity control persist.

With this review, we expect the reader to get some help in finding high-quality TMD materials with viable ALD processes for preparation. We also expect that the use of ALD as an important tool for the development of new 2D materials will be of more interest to researchers, thus furthering the development of the field.

AUTHOR INFORMATION

Corresponding Author

Jiaxu Yan − *Key Laboratory of Flexible Electronics (KLOFE) & Institute of Advanced Materials (IAM), Nanjing Tech University, Nanjing 211816, P. R. China; Changchun Institute of Optics, Fine Mechanics & Physics (CIOMP), Chinese Academy of Sciences, Changchun 130033, P. R. China; University of Chinese Academy of Sciences, Chinese Academy of Sciences, Beijing 100049, P. R. China;* orcid.org/0000-0002-9683-1188; Email: yanjiaxu@ciomp.ac.cn

Authors

Zhipu Li − *Key Laboratory of Flexible Electronics (KLOFE) & Institute of Advanced Materials (IAM), Nanjing Tech University, Nanjing 211816, P. R. China*

Xun Zhao − *Key Laboratory of Flexible Electronics (KLOFE) & Institute of Advanced Materials (IAM), Nanjing Tech University, Nanjing 211816, P. R. China*

Shiru Wu − *Key Laboratory of Flexible Electronics (KLOFE) & Institute of Advanced Materials (IAM), Nanjing Tech University, Nanjing 211816, P. R. China*

Min Lu − *Key Laboratory of Flexible Electronics (KLOFE) & Institute of Advanced Materials (IAM), Nanjing Tech University, Nanjing 211816, P. R. China;* orcid.org/0000-0003-3311-6491

Xiaoji Xie − *Key Laboratory of Flexible Electronics (KLOFE) & Institute of Advanced Materials (IAM), Nanjing Tech University, Nanjing 211816, P. R. China;* orcid.org/0000-0002-4830-1246

Complete contact information is available at: https://pubs.acs.org/10.1021/acs.cgd.3c01044

Notes

The authors declare no competing financial interest.

REFERENCES

(1) Yan, C. Y.; et al. 2D Group IVB Transition Metal Dichalcogenides. *Adv. Funct. Mater.* **2018**, *28*, 18.

(2) Wang, F.; et al. 2D library beyond graphene and transition metal dichalcogenides: a focus on photodetection. *Chem. Soc. Rev.* **2018**, *47*, 6296−6341.

(3) Tan, C. L.; Lai, Z. C.; Zhang, H. Ultrathin Two-Dimensional Multinary Layered Metal Chalcogenide Nanomaterials. *Adv. Mater.* **2017**, *29*, 25.

(4) Duan, X. D.; Wang, C.; Pan, A. L.; Yu, R. Q.; Duan, X. F. Two-dimensional transition metal dichalcogenides as atomically thin semiconductors: opportunities and challenges. *Chem. Soc. Rev.* **2015**, *44*, 8859−8876.

(5) Wen, W. Anisotropic Spectroscopy and Electrical Properties of 2D ReS2(1-x) Se2x Alloys with Distorted 1T Structure. *Small* **2017**, *13*, 1603788.

(6) Yu, Y. F.; et al. High phase-purity 1T'-MoS2- and 1T'-MoSe2-layered crystals. *Nat. Chem.* **2018**, *10*, 638−643.

(7) Nazif, K. N.; et al. High-specific-power flexible transition metal dichalcogenide solar cells. *Nat. Commun.* **2021**, *12*, 9.

(8) Nazif, K. N. *Transition Metal Dichalcogenides for Next-Generation Photovoltaics*. 2021.

(9) Kim, S. J.; et al. Fabrication of high-performance flexible photodetectors based on Zn-doped MoS2/graphene hybrid fibers. *J. Mater. Chem. C* **2017**, *5*, 12354−12359.

(10) Xu, Z.-Q.; Zhang, Y.; Wang, Z.; Shen, Y.; Huang, W.; Xia, X.; Yu, W.; Xue, Y.; Sun, L.; Zheng, C.; et al. Atomically thin lateral p−n junction photodetector with large effective detection area. *2D Mater.* **2016**, *3*, 041001.

(11) Berraquero, C. P., et al. Atomically thin quantum light emitting diodes. *arXiv*, March 29, 2016, arXiv:1603.08795, ver. 2. .

(12) Y Joe, A. et al. Electrically controlled emission from singlet and triplet exciton species in atomically thin light emitting diodes. *arXiv*, December 7, 2020, arXiv:2012.04022, ver. 1. .

(13) Gong, C. et al. Band alignment of two-dimensional transition metal dichalcogenides: application in tunnel field effect transistors. *arXiv*, August 4, 2013, arXiv:1308.0767, ver. 1. .

(14) Miikkulainen, V.; Leskela, M.; Ritala, M.; Puurunen, R. L. Crystallinity of inorganic films grown by atomic layer deposition: Overview and general trends. *J. Appl. Phys.* **2013**, *113*, 101.

(15) Hamalainen, J.; Ritala, M.; Leskela, M. Atomic Layer Deposition of Noble Metals and Their Oxides. *Chem. Mater.* **2014**, *26*, 786−801.

(16) Elam, J. W.; Routkevitch, D.; Mardilovich, P. P.; George, S. M. Conformal coating on ultrahigh-aspect-ratio nanopores of anodic alumina by atomic layer deposition. *Chem. Mater.* **2003**, *15*, 3507−3517.

(17) Zhou, H.; Bent, S. F. Fabrication of organic interfacial layers by molecular layer deposition: Present status and future opportunities. *Journal of Vacuum Science & Technology A* **2013**, *31*, 18.

(18) Knez, M.; Nielsch, K.; Niinisto, L. Synthesis and surface engineering of complex nanostructures by atomic layer deposition. *Adv. Mater.* **2007**, *19*, 3425−3438.

https://doi.org/10.1021/acs.cgd.3c01044
Cryst. Growth Des. 2024, 24, 1865−1879

(19) Marichy, C.; Bechelany, M.; Pinna, N. Atomic Layer Deposition of Nanostructured Materials for Energy and Environmental Applications. *Adv. Mater.* **2012**, *24*, 1017−1032.
(20) Parsons, G. N.; et al. Mechanisms and reactions during atomic layer deposition on polymers. *Coord. Chem. Rev.* **2013**, *257*, 3323−3331.
(21) Hatanpaa, T.; Ritala, M.; Leskela, M. Precursors as enablers of ALD technology: Contributions from University of Helsinki. *Coord. Chem. Rev.* **2013**, *257*, 3297−3322.
(22) Devi, A. Old Chemistries' for new applications: Perspectives for development of precursors for MOCVD and ALD applications. *Coord. Chem. Rev.* **2013**, *257*, 3332−3384.
(23) Xu, R. S.; Tao, Q.; Yang, Y.; Takoudis, C. G. Atomic layer deposition and characterization of stoichiometric erbium oxide thin dielectrics on Si(100) using (CpMe)(3)Er precursor and ozone. *Appl. Surf. Sci.* **2012**, *258*, 8514−8520.
(24) Nyns, L.; Delabie, A.; Swerts, J.; Van Elshocht, S.; De Gendt, S. ALD and Parasitic Growth Characteristics of the Tetrakisethylmethylamino Hafnium (TEMAH)/H(2)O Process. *J. Electrochem. Soc.* **2010**, *157*, G225−G229.
(25) Pilvi, T.; et al. Atomic layer deposition process with TiF4 as a precursor for depositing metal fluoride thin films. *Appl. Opt.* **2008**, *47*, C271−C274.
(26) Burton, B. B.; Kang, S. W.; Rhee, S. W.; George, S. M. SiO2 Atomic Layer Deposition Using Tris(dimethylamino)silane and Hydrogen Peroxide Studied by in Situ Transmission FTIR Spectroscopy. *J. Phys. Chem. C* **2009**, *113*, 8249−8257.
(27) Elam, J. W.; et al. Atomic layer deposition of tin oxide films using tetrakis(dimethylamino) tin. *Journal of Vacuum Science & Technology A* **2008**, *26*, 244−252.
(28) George, S. M.; Ott, A. W.; Klaus, J. W. Surface chemistry for atomic layer growth. *J. Phys. Chem.* **1996**, *100*, 13121−13131.
(29) Lee, B. H.; Yoon, B.; Abdulagatov, A. I.; Hall, R. A.; George, S. M. Growth and Properties of Hybrid Organic-Inorganic Metalcone Films Using Molecular Layer Deposition Techniques. *Adv. Funct. Mater.* **2013**, *23*, 532−546.
(30) Puurunen, R. L. Surface chemistry of atomic layer deposition: A case study for the trimethylaluminum/water process. *J. Appl. Phys.* **2005**, *97*, 52.
(31) Zhou, Z.; Xu, L.; Ding, Y.; Xiao, H.; Shi, Q.; Li, X.; Li, A.; Fang, G. Atomic layer deposition meets metal-organic frameworks. *Prog. Mater. Sci.* **2023**, *138*, 101159.
(32) Dong, H.; et al. In situ study of HfO2 atomic layer deposition on InP(100). *Appl. Phys. Lett.* **2013**, *102*, 4.
(33) Nakajima, A.; Khosru, Q. D. M.; Yoshimoto, T.; Kasai, T.; Yokoyama, S. High quality atomic-layer-deposited ultrathin Si-nitride gate dielectrics with low density of interface and bulk traps. *Appl. Phys. Lett.* **2003**, *83*, 335−337.
(34) Meng, X.; Byun, Y.-C.; Kim, H.; Lee, J.; Lucero, A.; Cheng, L.; Kim, J. Atomic Layer Deposition of Silicon Nitride Thin Films: A Review of Recent Progress, Challenges, and Outlooks. *Materials* **2016**, *9*, 1007.
(35) Chen, Y. *Epitaxial and Lateral Solid-Phase Crystallization of Complex Oxides*. 2019.
(36) Huang, Y.; Liu, L.; Zhao, W.; Chen, Y. Preparation and characterization of molybdenum disulfide films obtained by one-step atomic layer deposition method. *Thin Solid Films* **2017**, *624*, 101−105.
(37) Radisavljevic, B.; Radenovic, A.; Brivio, J.; Giacometti, V.; Kis, A. Single-layer MoS2 transistors. *Nat. Nanotechnol.* **2011**, *6*, 147−150.
(38) Ghatak, S.; Pal, A. N.; Ghosh, A. Nature of Electronic States in Atomically Thin MoS2 Field-Effect Transistors. *ACS Nano* **2011**, *5*, 7707−7712.
(39) Baugher, B. W. H.; Churchill, H. O. H.; Yang, Y. F.; Jarillo-Herrero, P. Intrinsic Electronic Transport Properties of High-Quality Monolayer and Bilayer MoS2. *Nano Lett.* **2013**, *13*, 4212−4216.
(40) Wang, F. L.; Stepanov, P.; Gray, M.; Lau, C. N. Annealing and transport studies of suspended molybdenum disulfide devices. *Nanotechnology* **2015**, *26*, 5.
(41) Wang, F. L.; et al. Ionic Liquid Gating of Suspended MoS2 Field Effect Transistor Devices. *Nano Lett.* **2015**, *15*, 5284−5288.
(42) Wang, Q. H.; Kalantar-Zadeh, K.; Kis, A.; Coleman, J. N.; Strano, M. S. Electronics and optoelectronics of two-dimensional transition metal dichalcogenides. *Nat. Nanotechnol.* **2012**, *7*, 699−712.
(43) Bertrand, P. A. SURFACE-PHONON DISPERSION OF MOS2. *Phys. Rev. B* **1991**, *44*, 5745−5749.
(44) Kam, K. K.; Parkinson, B. A. DETAILED PHOTOCURRENT SPECTROSCOPY OF THE SEMICONDUCTING GROUP-VI TRANSITION-METAL DICHALCOGENIDES. *J. Phys. Chem.* **1982**, *86*, 463−467.
(45) Mak, K. F.; Lee, C.; Hone, J.; Shan, J.; Heinz, T. F. Atomically Thin MoS2: A New Direct-Gap Semiconductor. *Phys. Rev. Lett.* **2010**, *105*, 4.
(46) Wu, S. F.; et al. Electrical tuning of valley magnetic moment through symmetry control in bilayer MoS2. *Nat. Phys.* **2013**, *9*, 149−153.
(47) Mak, K. F.; He, K. L.; Shan, J.; Heinz, T. F. Control of valley polarization in monolayer MoS2 by optical helicity. *Nat. Nanotechnol.* **2012**, *7*, 494−498.
(48) Tan, L. K.; et al. Atomic layer deposition of a MoS(2) film. *Nanoscale* **2014**, *6*, 10584−10588.
(49) Liu, L.; Huang, Y.; Sha, J.; Chen, Y. Layer-controlled precise fabrication of ultrathin MoS2 films by atomic layer deposition. *Nanotechnology* **2017**, *28*, 195605.
(50) Browning, R. Atomic layer deposition of MoS2 thin films. *Materials Research Express* **2015**, *2*, 035006.
(51) Liu, H.; et al. Atomic layer deposited 2D MoS2 atomic crystals: from material to circuit. *Nano Research* **2020**, *13*, 1644−1650.
(52) Jurca, T.; et al. Low-Temperature Atomic Layer Deposition of MoS2 Films. *Angew. Chem., Int. Ed. Engl.* **2017**, *56*, 4991−4995.
(53) Mattinen, M. Atomic Layer Deposition of Crystalline MoS2 Thin Films: New Molybdenum Precursor for Low-Temperature Film Growth. *Advanced Materials Interfaces* **2017**, *4*, 1700123.
(54) Shirazi, M.; Kessels, W. M. M.; Bol, A. A. Initial stage of atomic layer deposition of 2D-MoS2 on a SiO2 surface: a DFT study. *Phys. Chem. Chem. Phys.* **2018**, *20*, 16861−16875.
(55) Shen, C.; et al. Morphology-controlled MoS2 by low-temperature atomic layer deposition. *Nanoscale* **2020**, *12*, 20404−20412.
(56) Jin, Z.; Shin, S.; Kwon, D. H.; Han, S. J.; Min, Y. S. Novel chemical route for atomic layer deposition of MoS(2) thin film on SiO(2)/Si substrate. *Nanoscale* **2014**, *6*, 14453−14458.
(57) Pyeon, J. J.; et al. Wafer-scale growth of MoS2 thin films by atomic layer deposition. *Nanoscale* **2016**, *8*, 10792−10798.
(58) Zhang, T. High performance few-layer MoS2 transistor arrays with wafer level homogeneity integrated by atomic layer deposition. *2D Mater.* **2018**, *5*, 015028.
(59) Kim, D. H.; et al. Wafer-Scale Growth of a MoS2Monolayer via One Cycle of Atomic Layer Deposition: An Adsorbate Control Method. *Chem. Mater.* **2021**, *33*, 4099−4105.
(60) Yang, J.; Liu, L. Trickle Flow Aided Atomic Layer Deposition (ALD) Strategy for Ultrathin Molybdenum Disulfide (MoS2) Synthesis. *ACS Appl. Mater. Interfaces* **2019**, *11*, 36270−36277.
(61) Lopez-Sanchez, O.; Lembke, D.; Kayci, M.; Radenovic, A.; Kis, A. Ultrasensitive photodetectors based on monolayer MoS2. *Nat. Nanotechnol.* **2013**, *8*, 497−501.
(62) Wang, X. L.; et al. Chemical Vapor Deposition Growth of Crystalline Mono layer MoSe2. *ACS Nano* **2014**, *8*, 5125−5131.
(63) Saadi, F. H.; et al. Operand Synthesis of Macroporous Molybdenum Diselenide Films for Electrocatalysis of the Hydrogen-Evolution Reaction. *ACS Catal.* **2014**, *4*, 2866−2873.
(64) Wang, H. T.; et al. MoSe2 and WSe2 Nanofilms with Vertically Aligned Molecular Layers on Curved and Rough Surfaces. *Nano Lett.* **2013**, *13*, 3426−3433.
(65) Tang, H.; et al. Hydrothermal synthesis of 3D hierarchical flower-like MoSe2 microspheres and their adsorption performances for methyl orange. *Appl. Surf. Sci.* **2016**, *379*, 296−303.

https://doi.org/10.1021/acs.cgd.3c01044
Cryst. Growth Des. 2024, 24, 1865−1879

(66) Yang, X.; et al. Amorphous molybdenum selenide as highly efficient photocatalyst for the photodegradation of organic dyes under visible light. *Appl. Surf. Sci.* **2018**, *457*, 214−220.
(67) Zheng, X. T.; Yang, L. M.; Li, Y. B.; Yang, L. X.; Luo, S. L. Direct Z-scheme MoSe2 decorating TiO2 nanotube arrays photocatalyst for water decontamination. *Electrochim. Acta* **2019**, *298*, 663−669.
(68) Shelke, N. T.; Late, D. J. Hydrothermal growth of MoSe2 nanoflowers for photo- and humidity sensor applications. *Sens. Actuator A-Phys.* **2019**, *295*, 160−168.
(69) Charvot, J.; et al. Deposition of MoSe2 flakes using cyclic selenides. *RSC Adv.* **2021**, *11*, 22140−22147.
(70) Zazpe, R. Atomic Layer Deposition of MoSe2 Using New Selenium Precursors. *FlatChem.* **2020**, *21*, 100166.
(71) Tsang, C. F.; Ledina, M. A.; Stickney, J. L. Molybdenum diselenide formation using electrochemical atomic layer deposition (E-ALD). *J. Electroanal. Chem.* **2017**, *793*, 242−249.
(72) Wu, Y.; et al. A Self-Limited Atomic Layer Deposition of WS2 Based on the Chemisorption and Reduction of Bis(t-butylimino)bis-(dimethylamino) Complexes. *Chem. Mater.* **2019**, *31*, 1881−1890.
(73) Yang, H.; et al. Growth Mechanisms and Morphology Engineering of Atomic Layer-Deposited WS2. *ACS Appl. Mater. Interfaces* **2021**, *13*, 43115−43122.
(74) Kim, D. H.; Ramesh, R.; Nandi, D. K.; Bae, J. S.; Kim, S. H. Atomic layer deposition of tungsten sulfide using a new metal-organic precursor and H_2S: thin film catalyst for water splitting. *Nanotechnology* **2021**, *32*, 075405.
(75) Scharf, T.; et al. Growth, structure, and tribological behavior of atomic layer-deposited tungsten disulphide solid lubricant coatings with applications to MEMS. *Acta Mater.* **2006**, *54*, 4731−4743.
(76) Browning, R.; Kuperman, N.; Solanki, R.; Kanzyuba, V.; Rouvimov, S. Large area growth of layered WSe2films. *Semicond. Sci. Technol.* **2016**, *31*, 095002.
(77) Sharma, A.; et al. Low-temperature plasma-enhanced atomic layer deposition of 2-D MoS2: large area, thickness control and tuneable morphology. *Nanoscale* **2018**, *10*, 8615−8627.
(78) Cho, A.-J.; et al. Stepwise growth of crystalline MoS2 in atomic layer deposition. *J. Mater. Chem. C* **2022**, *10*, 7031−7038.
(79) Delabie, A.; et al. Low temperature deposition of 2D WS2 layers from WF6 and H2S precursors: impact of reducing agents. *Chem. Commun.* **2015**, *51*, 15692−15695.
(80) Groven, B.; et al. Two-Dimensional Crystal Grain Size Tuning in WS2 Atomic Layer Deposition: An Insight in the Nucleation Mechanism. *Chem. Mater.* **2018**, *30*, 7648−7663.
(81) Yeo, S.; et al. Low-temperature direct synthesis of high quality WS2 thin films by plasma-enhanced atomic layer deposition for energy related applications. *Appl. Surf. Sci.* **2018**, *459*, 596−605.
(82) Balasubramanyam, S.; et al. Area-Selective Atomic Layer Deposition of Two-Dimensional WS2 Nanolayers. *ACS Mater. Lett.* **2020**, *2*, 511−518.
(83) Ahn, W. Area-Selective Atomic Layer Deposition of MoS2 using Simultaneous Deposition and Etching Characteristics of MoCl5. *Physica Status Solidi (RRL) − Rapid Research Letters* **2021**, *15*, 2000533.
(84) Demirtaş, M.; Odacı, C.; Shehu, Y.; Perkgöz, N. K.; Ay, F. Layer and size distribution control of CVD-grown 2D MoS2 using ALD-deposited MoO3 structures as the precursor. *Materials Science in Semiconductor Processing* **2020**, *108*, 104880.
(85) Keller, B. D.; et al. Process Control of Atomic Layer Deposition Molybdenum Oxide Nucleation and Sulfidation to Large-Area MoS2Monolayers. *Chem. Mater.* **2017**, *29*, 2024−2032.
(86) Shi, M. L. Top-Down Integration of Molybdenum Disulfide Transistors with Wafer-Scale Uniformity and Layer Controllability. *Small* **2017**, *13*, 1603157.
(87) Dai, T.-J.; et al. Layer-controlled synthesis of wafer-scale MoSe2 nanosheets for photodetector arrays. *J. Mater. Sci.* **2018**, *53*, 8436−8444.
(88) Song, J.-G.; et al. Layer-Controlled, Wafer-Scale, and Conformal Synthesis of Tungsten Disulfide Nanosheets Using Atomic Layer Deposition. *ACS Nano* **2013**, *7*, 11333−11340.
(89) Romanov, R. I.; et al. Thickness-Dependent Structural and Electrical Properties of WS2 Nanosheets Obtained via the ALD-Grown WO3 Sulfurization Technique as a Channel Material for Field-Effect Transistors. *ACS Omega* **2021**, *6*, 34429−34437.

https://doi.org/10.1021/acs.cgd.3c01044
Cryst. Growth Des. 2024, 24, 1865−1879